Fmo5 plays a sex-specific role in goblet cell maturation and mucus barrier formation

Megan L. Schaller[1], Madeline L. Sykes[2], Joy Mecano[1], Sumeet Solanki[1], Wesley Huang[1,3,4] , Ryan J. Rebernick[4,5], Safa Beydoun[1], Emily Wang[1], Amara Bugarin-Lapuz[1], Yatrik M. Shah[1,6,#], Scott F. Leiser[1,6,#]

[1] Department of Molecular and Integrative Physiology, University of Michigan, Ann Arbor, MI, USA.

[2] Department of Molecular and Cellular Pathology, University of Michigan, Ann Arbor, MI, USA

[3] Department of Cellular and Molecular Biology, University of Michigan, Ann Arbor, MI, USA.

[4] Medical Scientist Training Program, University of Michigan, Ann Arbor, MI, USA.

[5] Department of Computational Medicine and Bioinformatics, University of Michigan, Ann Arbor, MI, USA.

[6] Department of Internal Medicine, University of Michigan, Ann Arbor, MI, USA.

# denotes co-corresponding authors

ABSTRACT

The intestine plays a key role in metabolism, nutrient and water absorption, and provides both physical and immunological defense against dietary and luminal antigens. The protective mucus lining in the intestine is a critical component of intestinal barrier function that when compromised, can lead to dysfunctional intestinal barriers that are a defining characteristic of inflammatory bowel disease (IBD), among other intestinal diseases. Here, we define a new role for the flavin-containing monooxygenase family of enzymes in maintaining a healthy intestinal epithelium. In nematodes, we find that *Cefmo-2* is necessary and sufficient for proper intestinal barrier function, intestinal actin expression, and is induced by intestinal damage. In mice, we utilize an intestine-specific, inducible knockout model of the prevalent gut Fmo (Fmo5) and find striking phenotypes within two weeks of knockout. These phenotypes include sex-dependent changes in colon epithelial histology, goblet cell localization and maturation factors, and mucus barrier formation. Each of these changes are significantly more severe in female mice, plausibly mirroring differences observed in some types of IBD in humans. Looking further at these phenotypes, we find increased protein folding stress in Fmo5 knockout animals and successfully rescue the severe female phenotype with addition of a chemical ER chaperone. Together, our results identify a new role for Fmo5 in the mammalian intestine and support a key role for Fmo5 in maintenance of ER/protein homeostasis and proper mucus barrier formation.

INTRODUCTION

The intestinal epithelium provides a barrier from environmental and microbial stress and its dysregulation is a hallmark of many intestinal diseases. The lining of the intestine is selectively permeable, forming a tight barrier to dietary antigens and luminal microbes while also taking up nutrients, electrolytes, and water. The colonic epithelium is protected by a bi-layer of mucus directly adjacent to epithelial cells. In a healthy organism, the physical and mucosal components form the intestinal barrier that prevents bacterial infiltration and intestinal cell damage[1]. Despite rapid epithelial cell turnover in the intestinal crypts[2], acute insults can lead to damage to the mucus and physical barriers. When damage to intestinal epithelial cells and intercellular junction complexes persists, it results in intestinal barrier dysfunction. Intestinal permeability, the translocation of bacteria and metabolic products into circulation, occurs in pathologic states including aging, inflammatory bowel disease (IBD), colitis, and ischemia[3]. Loss of intestinal barrier function can be exacerbated by environmental and systemic factors such as obesity, stress, and exposure to pathogens. Despite the relevance of preserving barrier function for maintaining gut homeostasis, the molecular mechanisms responsible for barrier damage during intestinal disease onset remain unclear.

The mucus barrier is composed of a dense inner layer with antimicrobial properties and a thick outer layer that is exposed to luminal contents[1]. Mucus maintains the intestinal barrier and is made solely by goblet cells, cup-shaped cells abundant in the colonic epithelium. Goblet cells constitutively synthesize mucins that, when secreted from storage vesicles, undergo biochemically-induced structural changes to expand, hydrate, and form an interconnected structure that makes up the inner layer of the colonic mucosal lining[4-6]. The absence of Muc2, the primary mucin in colonic goblet cells, leads to altered crypt morphology and impairments in goblet cell maturation and migration up the crypt[7]. These changes are detrimental to intestinal homeostasis.

The continuous requirement for colonic mucus production to maintain the barrier underscores the importance of the goblet cell's endoplasmic reticulum (ER) and unfolded protein response (UPR). The ER is tasked not only with efficiently folding the large Muc2 protein but also with promptly detecting and managing misfolded proteins. Impairments in goblet cell ER function can have detrimental effects on the formation and function of the mucus barrier. Dysfunction in mucin processing and exocytosis from goblet cells occurs more prevalently in patients with IBD (ulcerative colitis; UC)[8], negatively impacting mucus barrier function. Additionally, in mice with colitis and humans with ulcerative colitis (UC), the inner mucus layer is more penetrable to

bacteria, suggesting a failure in the antimicrobial function of the mucus barrier[9]. These failures can lead to stress from inflammation, changes in intestinal absorption, and damage to the intestinal epithelium[9,10].

Flavin-containing monooxygenases are ER-resident enzymes that play an important role in xenobiotic metabolism[11,12]. In previous studies, our lab discovered that *fmo-2* in *C. elegans* (*Cefmo-2*) is both necessary and sufficient to extend health and longevity following hypoxic and metabolic stress[11]. *Cefmo-2* is primarily expressed in the intestine of *C. elegans*, and the FMO family is highly conserved across taxa[13]. Through genetic manipulation and stress testing, we found that *Cefmo-2* is necessary to preserve intestinal integrity during environmental stress and aging in the worm. The function, structure, and homeostatic pathways of the nematode intestine are largely conserved, making it a useful model organism to investigate intestinal integrity and stress.

While the xenobiotic roles of FMOs have been well characterized, the endogenous roles of mammalian FMOs are still unclear. The mammalian homolog of *Cefmo-2*, Fmo5, is primarily expressed in the epithelial lining of the small intestine and colon, as well as in hepatocytes[14,15]. Fmo5 was recently reported as a regulator of metabolism and nutrient uptake using a constitutive KO mouse model[16]. However, little is known about the functional or cell autonomous role of FMO5 in the intestine. We developed an intestine-specific, inducible Fmo5 KO mouse to interrogate FMO function in the mammalian intestine. Here, through the establishment of this mouse model, we discover that Fmo5 plays a critical role in maintaining intestinal homeostasis. We show that disrupting Fmo5 in the adult intestine of mice causes significant perturbations to colonic crypt structure. These changes coincide with aberrant goblet cell localization and migration up the crypt after just 14 days of KO. We also find that intestinal Fmo5 is necessary to maintain mucosal barrier thickness in mice, in a sex-dependent manner. We rescue these impairments with an ER stress chaperone, supporting a role for Fmo5 in ER homeostasis. We propose a mechanistic role for Fmo5 in potentiating mucin processing within the ER that is imperative for mucosal barrier homeostasis in mice. These data highlight the exciting potential that Fmo5 could be exploited for therapeutic gain to benefit human health.

RESULTS

fmo-2 mediates intestinal integrity in *C. elegans*

Based on previous work showing that *Cefmo-2* is necessary and sufficient to improve stress resistance and longevity and that it is expressed primarily in the intestine[11,13], we were interested whether *fmo-2* affects worm intestinal integrity. To assess intestinal permeability in *C. elegans* we modified an assay commonly utilized in *Drosophila* called the Smurf assay[17]. This technique utilizes a non-absorbable dye that does not cross the intestinal barrier in healthy organisms. Following intestinal injury in worms, the dye leaks through intestinal cells into the body cavity (**Fig. 1A**). The dye is fluorescent, allowing us to quantify the amount of intestinal permeability of worms. Using wildtype worms, the intestinal permeability of *C. elegans* increases as the worm ages (**Fig. 1B**). This finding is consistent with previous work in *C. elegans*, *D. melanogaster*, and mammals showing a gradual decline in intestinal integrity as the organism ages. To test whether *Cefmo-2* plays a role in maintaining intestinal integrity, we used the Smurf assay with *fmo-2* knockout (KO) and *fmo-2* overexpressing (OE) worms. We found that worms without *fmo-2* display an increase in intestinal permeability by day 6 of adulthood (**Fig. 1C, D**). By day 10 of adulthood, wild-type worms have equaled the increase in permeability in *fmo-2* KO animals whereas *fmo-2* OE worms have less permeability than wildtype worms (**Fig.1E, F**). This result suggests that FMO-2 is critical in maintaining intestinal integrity during aging.

To test whether *fmo-2* is also involved in responding to intestinal damage, we utilized dextran sodium sulfate (DSS) to induce intestinal injury[18]. Employing a *fmo-2* transcriptional reporter worm strain, we find that *fmo-2* is significantly induced in worms following 20 hours of exposure to 5% DSS (**Fig. 1G, H**). Combined with previously published results from our lab and others, where *fmo-2* is induced with exposure to other environmental stressors (dietary restriction, hypoxia, pathogens), this finding is consistent with a model of FMO-2 playing a role in broad environmental stress response[11,19]. To assess the importance of *fmo-2* in maintaining the physical integrity of intestinal cells in *C. elegans*, we used an ACT-5 translational reporter worm strain and RNA interference (RNAi) to knockdown *fmo-2*. ACT-5 is the singular actin protein in the intestinal cells of *C. elegans*, where it makes up the structure of microvilli in the intestinal lumen[20]. Knocking out ACT-5 in worms is embryonically lethal, and the amount of ACT-5 is directly related to the integrity of intestinal cells where lower levels of ACT-5 lead to increased permeability[20]. We find significantly decreased levels of ACT-5 protein in worms when *fmo-2* is knocked down with RNAi (**Fig. 1I, J**), suggesting *fmo-2* is necessary for maintaining intestinal integrity in the basal state.

Fmo5 plays a sex-dependent role in maintaining intestinal crypt architecture

There are five FMOs in *C. elegans* and mammals. The phylogenic analysis of active site sequences of FMO proteins suggests that all *C. elegans* FMOs are most closely related to mammalian Fmo5[21]. Fmo5 in mammals is primarily found in the liver and the epithelium of the small intestine and colon (**Fig. 2A**)[15]. To explore the conserved role of *Cefmo-2*/Fmo5 we generated a Fmo5 floxed mouse line. Building on our finding that *fmo-2* is necessary for a healthy intestine in *C. elegans*, we crossed the Fmo5 floxed mouse line with an intestinal epithelium-specific, inducible VillinER^{T2} cre line to generate mice with an intestine-specific, tamoxifen-inducible Fmo5 KO (VillinER^{T2} cre^{+}; Fmo5$^{fl/fl}$) (**Fig. 2B**). To validate this mouse line, we treated VillinER^{T2} cre^{+}; Fmo5$^{fl/fl}$ mice with tamoxifen (100 mg/kg body weight IP injection, 1 x 5 days) to make Fmo5$^{-/-}$ mice and waited 14 days (2-3 epithelium turnovers) before collecting the colonic epithelium and isolating RNA and protein. Gene expression analysis using RT-qPCR revealed significantly less Fmo5 expression in Fmo5$^{-/-}$ mice when compared to Fmo5$^{+/+}$ mice that also received tamoxifen treatment (**Fig. 2C**). To confirm that the Fmo5 protein was not present in these mice, we measured Fmo5 protein levels in the colonic epithelium and the liver. We show (**Fig. 2D**) that there is no measurable Fmo5 protein in the colon of Fmo5$^{-/-}$ mice, and that Fmo5 protein levels are maintained in the liver, validating the tissue specificity of this KO mouse model.

Histological analysis of the colonic epithelium in these mice revealed significantly shorter crypts and a dysregulation in the uniformity of crypt structure at 14 days of knockout in female Fmo5$^{-/-}$ mice, as compared to their Fmo5$^{+/+}$ littermates. We were surprised to find that this crypt shortening and dysregulation was not readily present in male Fmo5$^{-/-}$ mice, where we find elongated crypts when compared to male Fmo5$^{+/+}$ mice. This is intriguing, as intestinal health and the progression of some gastrointestinal diseases in humans varies based on sex[22].

The entirety of the colonic epithelium is replaced every 4-5 days in mammals by terminally differentiating cells generated from stem cell pools that reside at the bottom (basolateral side) of crypts[23]. To determine if Fmo5 plays a role in maintaining the structure of crypts after they are already formed and/or if Fmo5 is necessary for epithelial cell turnover in the colon, we performed H&E staining in Fmo5$^{+/+}$ and Fmo5$^{-/-}$ mice at 3-, 7-, and 10- days following tamoxifen treatment. After 3 days of knockout, we do not see distinct differences in epithelial architecture between female Fmo5$^{+/+}$ and Fmo5$^{-/-}$ mice. However, 7 days after the removal of Fmo5 from the intestine there is a loss of crypt uniformity in female Fmo5$^{-/-}$ mice, where crypts appear to be

stacked on top of one another and the epithelium starts to become “disheveled” (**Fig 2G**). At day 10 of KO, the uniformity of crypt architecture remains lost in these mice.

Similar to what we observe in females, there are no differences between male Fmo5$^{+/+}$ and Fmo5$^{-/-}$ mice at day 3 and 7 of KO. At 10 days post knockout, male Fmo5$^{-/-}$ mice have significantly longer crypts than both their wildtype littermates and Fmo5$^{-/-}$ mice at days 3 and 7 (**Fig. 2H, J**). This could suggest that the male epithelium reaches a steady state of crypt length when compensating for the loss of Fmo5, whereas female Fmo5$^{-/-}$ mice are still experiencing a restructuring of their epithelial architecture at this timepoint. The lack of gross changes in the epithelial structure of both female and male Fmo5$^{-/-}$ mice after 3 days of KO plausibly suggests that Fmo5 is not necessary for overall cell survival in an acute sense, but rather that subsequent turnover and development of the epithelium is altered when Fmo5 is lost.

Female Fmo5$^{-/-}$ mice have impaired goblet cell localization and maturation

The intestinal epithelium is made up of a heterogenous collection of cells including enteroendocrine, absorptive, and secretory cell types each performing distinct functions to maintain homeostasis[24,25]. To explore if secretory or absorptive cell types were more impacted by the loss of Fmo5, we first measured the expression of absorptive genes (Slc2a5 and Alpi) within the epithelium in Fmo5$^{+/+}$ and Fmo5$^{-/-}$ mice after 14 days of KO. We found no significant differences in absorptive cell markers (**Supplemental Fig. 1A**). We next measured secretory cell markers and found that the expression of the goblet cell genes, Muc2 and Tff3, were significantly increased in female Fmo5$^{-/-}$ mice but not in male Fmo5$^{-/-}$ mice (**Fig. 3A**). We then asked whether the protein levels of Muc2 were different in these mice. Muc2 is the primary mucin synthesized and stored in goblet cells, until it is released to form mucus that makes up the bi-layered mucus barrier that protects the epithelial lining of the colon. Immunofluorescence (IF) staining of Muc2 revealed altered localization of goblet cells in female Fmo5$^{-/-}$ mice, where goblet cells are clustered at the bottom of the crypt rather than being spread throughout the crypt as we observe in Fmo5$^{+/+}$ mice (**Fig. 3B**).

Within the crypt structure of the colon, some cell types differentiate and mature as they migrate up the crypt toward the luminal space[26]. To determine if Fmo5$^{-/-}$ mice have an impairment in overall epithelial cell migration, we injected Fmo5$^{+/+}$ and Fmo5$^{-/-}$ mice with EdU, a fluorescent label that gets taken up during DNA synthesis, and waited 24 hours before collecting the colon for histological analysis (**Fig. 3C**). We then performed IF staining of Muc2 (magenta) and EdU (green) (**Fig. 3D**) to visualize the location of cells that were actively replicating when EdU was

injected 24 hours prior. We measured the distance up the crypt that the EdU+ cells had migrated within 24 hours and normalized that distance to individual crypt length (**Fig. 3E**). When the shorter crypt length of female Fmo5$^{-/-}$ mice was controlled for, there were no difference in the migration distance of EdU+ cells up the crypt between female Fmo5$^{+/+}$ and Fmo5$^{-/-}$ mice at 24 hours. This supports that overall epithelial cell migration is not altered in Fmo5$^{-/-}$ mice, but rather goblet cell migration is impaired. This is intriguing, as goblet cells mature as they migrate up the crypt towards the lumen of the intestine, and their maturity is imperative for the ability to properly secrete mucin in response to systemic cues[27]. In support of this, we find no difference in absorptive or progenitor cell expression (Hes-1, Atoh-1) in our mice, suggesting the lack of goblet cells in the upper crypt is not due to a decrease in secretory cell lineage differentiation but rather an impairment in maturation (**Supplementary Fig. 1B**). To further probe this model, we measured the expression of genes associated with goblet cell maturation in epithelial colon scrapes from female Fmo5$^{+/+}$ and Fmo5$^{-/-}$ mice 14 days following tamoxifen treatment. We find that Fmo5$^{-/-}$ mice have significantly lower expression of genes necessary for goblet cell maturity, Klf4, Spdef, and Glfi1 (**Fig. 3F**)[27,28]. This finding, in conjunction with the spatial impairments of goblet cells within the crypts that we see in female Fmo5$^{-/-}$ mice, supports a role for Fmo5 in goblet cell development and maturity.

Fmo5 is necessary for mucus production and mucus barrier thickness in female mice

After Muc2 protein is synthesized in the goblet cell, the protein undergoes complex folding and N-glycosylation within the ER[29] before moving to the golgi apparatus to be O-glycosylated[30]. Following post-translational modification, the mucin protein is then stored in secretory vesicles in the cup-shaped region of the cell to await release into the crypt or luminal space. Given that goblet cell localization and maturity is impaired in female Fmo5$^{-/-}$ mice, we next wanted to test the functional capacity of goblet cells to produce mucus. AB/PAS staining of mucus within the crypts of Fmo5$^{+/+}$ and Fmo5$^{-/-}$ mice revealed a decrease in overall mucus production from goblet cells (GC) within female Fmo5$^{-/-}$ crypts. This suggests that the spatial and migration impairments of GCs in these mice are sufficient to negatively impact their capacity to produce mucus (**Fig. 4A**). We observe a subtle reduction in mucus within the crypts of male Fmo5$^{-/-}$ mice, although not to the severity that we see in females. When assessing mucus production temporally, we find that female Fmo5$^{-/-}$ mice have similar levels of mucus within the crypt as their wildtype littermates at day 3 post-tamoxifen treatment. By day 7, female KO mice begin to show dysregulated crypt organization along with noticeably less mucus within the epithelium (**Fig.**

4B). At day 10 of KO, female Fmo5$^{-/-}$ mice display shorter crypts, similar to what we see at day 14 of KO. This is coupled with a lack of mucus in the upper half of the crypts, whereas in Fmo5$^{+/+}$ mice we see mucus-filled goblet cells spread from the apical to basolateral borders of the crypts. Like females, we see no differences in mucus production in male Fmo5$^{-/-}$ mice at day 3 of KO (**Fig. 4C**). At day 7 post-tamoxifen, there is a slight reduction in mucus present within the crypts of male Fmo5$^{-/-}$ mice when compared to wildtype. This reduction is also present at day 10 and 14 of KO, where there is mild loss of mucus sporadically among crypts (**Fig. 4C**).

In histology slide preparation the colon is cut open lengthwise and rinsed in PBS before being rolled and embedded in paraffin. During this type of processing, the layers of mucus that make up the mucus barrier are washed away while the mucus located within the goblet cells of crypts are preserved. Interestingly, we observed that 5/5 of female Fmo5$^{-/-}$ mice at day 3 of KO have a layer of mucus adhered to the epithelium that was not washed away during processing. Additionally, an attached mucus layer is present in 4/5 female Fmo5$^{-/-}$ mice at day 7 of KO, something we did not find in any Fmo5$^{+/+}$ or male Fmo5$^{-/-}$ mice. The explanation for this observation is unclear but could involve structural differences in the mucus produced by female Fmo5$^{-/-}$ mice, causing greater adherence of mucus to the epithelium immediately after Fmo5 loss. Using Carnoy's Fixative solution that preserves the mucus barrier (**Fig. 4C**), we find a significantly thinner inner mucus barrier in female Fmo5$^{-/-}$ mice at day 14 of KO when compared to wildtype and male Fmo5$^{-/-}$ mice (**Fig. 4D, E**). Overall, these results are suggestive of both impaired mucus production within crypts and the necessity of Fmo5 to maintain mucus barrier thickness in female mice.

Mucus impairments in Fmo5$^{-/-}$ mice are not likely caused by dysbiosis

The mucus barrier in the colon is imperative for preventing microbes and bacterial metabolites in the microbiota from coming into physical contact with the epithelium. A culmination of physical, chemical, and antimicrobial qualities of the mucus making up the barrier establishes an environment that is not cohesive to microbe survival. However, when mucus barrier function fails during disease, bacteria and microbes can cause damage to the epithelial lining and eventually translocate into circulation, triggering an immune response. Some species of bacteria that make up the microbiota can break down mucus for energy, further exacerbating mucus barrier impairment. When the balance of beneficial and harmful bacteria abundance in the microbiota is lost, dysbiosis can occur, and is purported as one of the potential drivers for GI disease onset.

To determine if the damaged epithelium we observe in female Fmo5$^{-/-}$ mice is caused by dysbiosis, we utilized 16s rRNA sequencing of feces from Fmo5$^{+/+}$ and Fmo5$^{-/-}$ mice to identify bacterial species making up their microbiome. We found no significant changes in the microbial populations of Fmo5$^{-/-}$ animals compared to their littermate controls after 13 days of KO (**Fig. 5A**), indicating that dysbiosis is not likely the primary cause of the intestinal phenotype. To further explore if dysbiosis was occurring in Fmo5$^{-/-}$ mice, we treated Fmo5$^{+/+}$ and Fmo5$^{-/-}$ mice with broad-spectrum antibiotics (Gentamycin, Ampicillin, Neomycin, Penicillin, Streptomycin) in their drinking water. This treatment was coupled with additional Vancomycin and Metronidazole, or PBS (control) gavages every 2-3 days to drastically reduce the diversity of their microbiota (**Fig. 5B**). To account for any initial differences in the microbiota between cages, we normalized the microbiota of mice prior to tamoxifen treatment. After 14 days of KO (9 days of antibiotic treatment), we used H&E staining to assess differences in epithelial architecture with antibiotics. We find that antibiotic treatment did not rescue crypt damage or goblet cell alterations in female Fmo5$^{-/-}$ mice (**Fig. 5C, D, E**). When comparing crypt structure in Fmo$^{+/+}$ and Fmo5$^{-/-}$ mice we see that both wildtype groups and male Fmo5$^{-/-}$ mice experience crypt shortening with the addition of antibiotics whereas female Fmo5$^{-/-}$ crypts are not shorter than they are without antibiotics. We speculate that this could be due to the loss of beneficial bacteria and that female Fmo5$^{-/-}$ are already so affected that any greater loss of crypt architecture might not be cohesive to survival. Despite the lack of evidence that the Fmo5$^{-/-}$ phenotype is rooted in dysbiosis, it is still possible that female Fmo5$^{-/-}$ mice interact differently with homeostatic bacteria within the gut.

The ER chaperone TUDCA rescues crypt dysregulation and mucus barrier impairment in female Fmo5$^{-/-}$ mice

The capacity of the ER to properly fold the large Muc2 protein during mucin synthesis is imperative for maintaining a healthy intestinal mucus barrier. To test for changes in ER stress response, we used RT-qPCR to measure the level of spliced XBP1, a key transcription factor of the UPR^{ER}. We find that total XBP1 levels are significantly decreased in female Fmo5$^{-/-}$ mice (**Fig. 6A**). We also find less of the spliced, active form of XBP1 contributing to a significantly lower ratio of spliced to total XBP1 with Fmo5$^{-/-}$ (**Fig. 6A)**. This result could represent a decreased response to ER stress in mice without Fmo5. Considering how imperative it is for goblet cells to effectively complete the many steps involved in producing and secreting mucus, the ER of GCs has evolved to include an additional ER-UPR arm in AGR2/IRE-1β that is specifically sensitive to Muc2[31,32]. We measured protein levels of the chaperone for this arm, AGR2, and find that AGR2 levels are significantly higher in Fmo5$^{-/-}$ mice than wildtype (**Fig. 6B,**

C). To explore if ER stress causes the crypt and mucus barrier defects that we see in female Fmo5$^{-/-}$ mice, we treated Fmo5$^{+/+}$ and Fmo5$^{-/-}$ mice with the chemical ER chaperone Tauroursodeoxycholic acid (TUDCA). TUDCA or PBS (control) was given (500mg/kg/day, IP injection) 7 days prior to and during tamoxifen treatment, in addition to 15 days following KO (**Fig. 6D**). H&E staining to assess crypt architecture revealed a complete rescue of crypt length in female Fmo5$^{-/-}$ mice with TUDCA treatment, compared to Fmo5$^{-/-}$ mice given PBS (**Fig. 6F, E**). Mucus production from goblet cells within the crypt is also restored with TUDCA treatment, where Fmo5$^{-/-}$ mice given TUDCA have comparable, if not increased, amounts of inter-crypt mucus present (**Fig. 6G**). Additionally, we find that TUDCA treatment in Fmo5$^{-/-}$ mice completely restores inner mucus barrier thickness when compared to Fmo5$^{-/-}$ mice without TUDCA (**Fig. 6H, I**). The ability of an ER chaperone to improve crypt and mucus defects in mice without Fmo5 suggests that the underlying cause of these defects involves protein folding and/or the ER stress response.

DISCUSSION

Together, our results support a model in which FMOs play a conserved, integral role in maintaining intestinal homeostasis. In *C. elegans,* we show that *fmo-2* is necessary to maintain structural integrity and barrier function in the intestine (**Fig. 1**). Building upon this, to define the conserved role of FMOs in maintaining intestinal homeostasis, we generated an inducible, intestine-specific mouse model of mammalian Fmo5. Characterization of this mouse line revealed a sex-dependent role for Fmo5 in the maintenance of epithelial architecture in the colon (**Fig. 2E**). Our results also demonstrate the necessity of Fmo5 for goblet cell localization and Muc2 expression, leading to thinning of the mucosal barrier with loss of Fmo5 in mice (**Fig. 4D, E**). High demand on the goblet cell ER to process mucins and evidence of ER stress marker activation in KO animals led us to hypothesize that Fmo5 is essential to maintain ER homeostasis. This hypothesis is supported by the rescue of crypt architecture and mucus barrier thickness with the addition of the ER chaperone, TUDCA (**Fig. 6F, H**). Our results 1) support a new role for FMO5 in maintaining intestinal ER homeostasis, and 2) introduce a new mouse model of intestinal dysfunction. Overall, this work highlights the importance of Fmo5 in maintaining a healthy intestine in mice.

Maintaining the physical integrity of cells making up the intestinal epithelium is critical for preserving intestinal homeostasis and function. Histomorphological assessment of crypt architecture is a useful tool when diagnosing GI disease in a clinical setting, and its relevance to disease spans into mammalian models[33,34]. Studies show that shortening of crypts in the colon

(crypt atrophy), crypt distortion, and crypt loss are all present in mice with IBD and these alterations have a direct impact on epithelial health[35]. Additionally, crypt shortening and disarray along with crypt branching and mucin depletion are all diagnostic features of ulcerative colitis (UC) in humans[36-39]. These are all characteristics that we see in the colonic epithelium of female Fmo5$^{-/-}$ mice, leading us to hypothesize that Fmo5 plays a protective role in GI disease onset. The severity of crypt shortening that we report (**Fig. 2E**) is comparable with the severity of crypt shortening found in mice treated with DSS[35]. This is intriguing, as Fmo5 has not been identified as a regulator of epithelial maintenance. Crypt lengthening in male Fmo5$^{-/-}$ mice could be attributed to crypt epithelial hyperplasia or crypts elongating to increase cell number and surface area to maintain epithelial function with Fmo5$^{-/-}$ (**Fig. 2F**)[40,41]. We also find that the loss of structural homeostasis in the colon of female Fmo5$^{-/-}$ mice compounds with each epithelial turnover, resulting in dramatic crypt distortion by 14 days post-KO (**Fig. 2G**). From this, we conclude that Fmo5 is necessary for the formation of a healthy epithelium in the colon. Additional investigation is needed to determine if female mice without Fmo5 are also hypersusceptible to intestinal cues or intestine-specific stress.

Studies show that altered epithelial architecture in mice can result from defects in cell differentiation and migration, where cells are unable to terminally differentiate or effectively migrate up the crypt toward the lumen of the intestine[26]. We find that goblet cells in female Fmo5$^{-/-}$ mice are clustered toward the bottom of the crypt rather than being spread uniformly throughout (**Fig. 3B**). This is intriguing, as mice lacking the primary mucin in colonic goblet cells (Muc2) exhibit altered crypt morphology and have impairments in goblet cell migration up the crypt. These data are consistent with Scott *et al.,* who observed decreased goblet cell number in a ubiquitous constitutive male Fmo5$^{-/-}$ mouse[42]. Multiple factors necessary to drive goblet cell maturation and migration have been identified (Klf4, Spdef, Glfi1), and several studies link impairments in these with the development of IBD[28,39]. One phenotype specifically attributed to cases of UC in humans, rather than IBD as a whole, is a loss of mucin-producing goblet cells in the top half of the crypt coupled with depleted mucus barrier[37,43-45]. GC clustering and loss of upper crypt goblet cells in unchallenged female Fmo5$^{-/-}$ mice (**Fig. 3B**) is also consistent with published models of DSS-induced colitis, where GC dysfunction is attributed to decreased GC maturation factors (also found in Fmo5$^{-/-}$ mice (**Fig. 3F**))[28,39]. Additionally, the lack of differences in absorptive or progenitor cell expression in our mice further support that maturation is the likely defect (**Supplementary Fig. 1B**). These findings, coupled with an increase in GC gene expression (Muc2, Tff3) that we suspect is compensatory (**Fig. 3A)**, suggest that Fmo5 contributes to GC regulation in female mice.

Maintaining a protective mucus barrier is the culmination of a range of structural, functional, and biochemical processes. Here we show that intestinal Fmo5 is necessary for proper mucus production within colonic crypts and mucus barrier maintenance in female mice (**Fig. 4**). Previously published studies show that impairments in Muc2 folding, defects in O- and N-glycosylation, and aggregation of the non-glycosylated form of Muc2 in mice each cause hyper-susceptibility to colitis coupled with aberrant goblet cell function[46]. It is likely that one of more of these protein processing impairments occur in Fmo5$^{-/-}$ females, given that **1)** Fmo5 resides in the ER membrane, and **2)** we find evidence of ER stress with increased levels of the mucin-specific chaperone, AGR2 (**Fig. 6B**). A previous study showed that the BiP/IRE-1α arm of the UPR senses a wide variety of ligands that cause ER stress but does not respond to excess Muc2 presence[31]. A mucin-sensitive UPR^{ER} arm made up of AGR2 and IRE1β is hypothesized to take on the responsibility for the folding of mucins in goblet cells[31,47]. A study by Grey *et al*. reports that in basal states, cells expressing IRE1β had increased XBP1 splicing, but when challenged with the ER stress-inducer, thapsigargin (Tg), IRE1β blunted IRE1α activity resulting in significantly decreased XBP1 splicing, perhaps as a protective mechanism[47]. This may prevent the ER stress response from overwhelming the ER in mucosal epithelial cells. Our findings are consistent with this, as we show increased IRE1β protein levels in female Fmo5$^{-/-}$ mice along with significantly lower spliced XBP1 levels (**Fig. 6A**). We hypothesize that loss of Fmo5 leads to ER stress, triggering IRE1β activation and reduced XBP1 splicing. Treating mice with the chemical ER chaperone TUDCA was sufficient to rescue this ER stress and prevent crypt architecture dysregulation and mucosal impairments in female Fmo5$^{-/-}$ mice (**Fig. 6E-G**). While further exploration of this system is necessary to identify the molecular mechanism of how Fmo5 plays into ER stress regulation, our results imply that goblet cell and mucus barrier defects in female Fmo5$^{-/-}$ mice are caused by altered protein folding and/or ER stress. This establishes a role for Fmo5 in maintaining mucosal barrier integrity and intestinal homeostasis in mice through ER stress protection.

Here we show the highly conserved enzyme, FMO5, when disrupted in mice, exhibits many characteristics of chronic GI disease but only in female mice. This is a striking sex difference that parallels that observed in humans, despite no clear linkage between Fmo5 and GI disease pathogenesis. The mechanism underlying sexual dimorphism in GI disease is largely unclear, and this model provides a unique opportunity within the field to dissect the cellular mechanisms. Both the prevalence and progression of IBD differs in humans based on sex, where women are more likely to develop Crohn's Disease (CD) and men are more susceptible to ulcerative colitis (UC)[22]. One study found that post age 45, females are up to 32% less likely to be diagnosed

with UC when compared to males[48]. This is coupled with another report showing that Fmo5 expression was down-regulated in a UC dataset[49]. Interestingly, we find no differences in Fmo5 expression levels in the intestinal epithelium between female and male mice at 1, 3, or 6 months of age (**Supplemental Fig. 1C**). This fails to support the simple explanation that female mice are more susceptible to Fmo5 loss simply because they have higher intestinal Fmo5 levels. We speculate that Fmo5 could be interacting with sex hormones in some way to provide protection from intestinal dysfunction in female mice.

Together, this work describes a previously unidentified role for Fmo5 in maintaining intestinal integrity and mucosal barrier homeostasis. Future directions for this project include further clarifying the cellular mechanism of how intestinal Fmo5 influences GI disease onset, with the overall goal to utilize the resulting data to improve therapeutic treatment for GI diseases. There is also a need to identify the cellular mechanism(s) by which acute loss of Fmo5 leads to defects in goblet cell maturation and migration and if they include alterations in metabolic environment. Future investigation is also warranted to determine if there are any changes to the biochemical components of mucus produced in mice without FMO5 and how those changes influence mucus barrier integrity.

MATERIALS AND METHODS

Worm Strain and Maintenance

Wildtype N2, KAE9 (*fmo-2* OE), VC1668 (*fmo-2* KO), ELT-60 (ACT-5::GFP), and LZR1 (*fmo-2p::MC*) strains of *C. elegans* were age synchronized by timed egg lay prior to use. Strains were grown and maintained on solid nematode growth media (NGM) throughout their lifespan. The nematodes were fed *E. coli* OP50 throughout life except where RNAi (*E. coli* HT115 *act-5*, *fmo-2*, and Control Empty Vector) were fed instead. All experiments were performed at 20°C.

Smurf Assay

Wildtype, *fmo-2* KO, and *fmo-2* OE worms were synchronized and fed OP50 *E. coli* bacteria dyed with 0.10% wt/vol. Erioglaucine disodium salt (Sigma Aldrich, FD&C, Blue #1 PD1100, powder). At each day of analysis, worms were placed on a 3% agarose pad on a glass slide, and 1M sodium azide was used to induce paralysis before imaging using a Leica fluorescent microscope. Fluorescent intensity of each worm was quantified using ImageJ.

DSS Assay

fmo-2p::mCherry worms were age synchronized and fed with OP50 *E. coli* until day 1 of adulthood. They were then incubated in M9 wash solution with OP50+/- 5% dextran sodium sulfate (DSS) for 20 hours at 20°C prior to imaging. Worms were placed on a 3% agarose pad on a glass slide, and 1M sodium azide was used to induce paralysis before imaging using a Leica fluorescent microscope. Fluorescent intensity of each worm was quantified using ImageJ.

Mouse Line Generation

The Fmo5$^{fl/fl}$ mouse line was generated in collaboration with the Transgenic Animal Model Core of the University of Michigan's Biomedical Research Core Facilities. Briefly, purified DNA was microinjected into fertilized eggs obtained by mating (C57BL/6 X SJL)F1 or C57BL/6 female mice with (C57BL/6 X SJL)F1 male mice. Pronuclear microinjection was performed as described[50]. Fmo5$^{fl/fl}$ were then crossed into the intestine-specific, inducible VillinER^{T2} cre mouse line and backcrossed a minimum of 5 generations prior to using for experiments.

Mouse Husbandry

All mice used in this study were 8-12 week old VillinER^{T2} cre^{+}; Fmo5$^{fl/fl}$ and Fmo5$^{fl/fl}$ female and male mice in a C57Bl/6 background. Littermate controls were used whenever possible. All mice were housed in the pathogen-free Unit for Laboratory Animal Management at the University of Michigan. Mice were kept under a 12-hour light/12- hour dark cycle and standard chow and water were provided *ad libitum.* All animal studies were conducted in accordance with Association for Assessment and Accreditation of Laboratory Animal Care International guidelines and approved by the University Committee on the Use and Care of Animals at the University of Michigan.

Tamoxifen Treatment

Mice were given intraperitoneal injection of 100 mg/kg Tamoxifen (MP Biomedical) in corn oil once daily for 5 days. Mice were weighed daily during treatment to monitor health and were housed by genotype and sex. The 5th and final day of injection was considered Day 0 of Fmo5 knockout for all experiments in this study.

Histology

To prepare samples for general histological analysis, the colon was removed at necropsy and opened lengthwise. The colon was rinsed in 1x PBS and rolled to create a swiss roll[51]. Samples were incubated in 10% buffered formalin phosphate (Fisher Chemical) overnight at room

temperature before being moved to 70% ethanol until further processing. Tissues were dehydrated by paraffin wax embedding and sliced into 4 μm sections[52].

For mucus barrier histological analysis, upon euthanasia the colon was removed and kept intact. Horizontal cuts were made above and below a fecal pellet midway down the colon and the sample was immediately placed into to Carnoy's Fixative (Spectrum) to preserve the mucus barrier[53]. Samples were incubated overnight at room temperature in Carnoy's solution prior to being moved to 70% ethanol and stored at 4°C until paraffin embedding. Embedding and sectioning was performed using the same method as described above.

Immunofluorescence

Slides were deparaffinized using xylene and rehydrated using washes of 100%, 95%, and 80% ethanol at room temperature. Samples underwent antigen retrieval in sodium citrate buffer with a pH of 6.0 (Thermo Scientific) at 100° for 20 minutes. Samples were blocked with goat serum and incubated in Muc2 primary antibody (Proteintech) overnight at 4° at a concentration of 1:1000. The following day, slides were rinsed and incubated in secondary antibody (Anti-GFP, Invitrogen) for 1 hour at room temperature (RT) at 1:500 concentration. Following incubation, samples were washed and cover slips were mounted using Prolong Gold with Dapi (Fisher Chemical).

EdU Injection and Staining

Mice were given intraperitoneal injection of 25 mg/kg of EdU (5-ethynyl-2'-deoxyuridine, Invitrogen) dissolved in 1x PBS on Day 13 of knockout. Exactly 24 hours later, mice were euthanized by $C0_2$ inhalation, and intestinal tissue was collected for histological analysis. Samples were deparaffinized using xylene and rehydrated using washes of 100%, 95%, and 75% ethanol at room temperature. Immunofluorescence staining as described above was performed until after the secondary incubation step. Slides were then incubated in 0.5% Triton X-100/PBS for 20 minutes at RT and EdU staining was performed using a Click-iT EdU Kit (Invitrogen) following the included protocol. Briefly, slides were incubated in fresh Click-iT reaction cocktail for 30 minutes at RT in the dark. Coverslips were mounted using Prolong Gold with Dapi (Fischer Scientific). Slides were scanned into the computer using a slide scanner and imaged for analysis.

Antibiotic Treatment

Prior to tamoxifen treatment, 8-12 week old female and male $Fmo5^{+/+}$ and $Fmo5^{-/-}$ mice underwent microbiota normalization by collecting, mixing, and redistributing the bedding of all

cages involved in the experiment every other day for 2 weeks. Following microbiota normalization, mice were given IP injections of tamoxifen (100 mg/kg of body weight, MP Biochemical) for 5 days. From days 5-14 of knockout, mice were provided an antibiotic cocktail or water (control) in their water supply. The antibiotic treatment consisted of gentamycin at (500 mg/L), ampicillin (1 g/L), neomycin (1 g/L), penicillin (100 U/L), and streptomycin (200 mg/L). The mice were also given a 150 μL gavage consisting of vancomycin (1 mg/mL) and metronidazole (0.5 mg/mL) or PBS (control) every other day starting on day 5 of KO. Mice were euthanized at day 14 of knockout and proximal colon samples were collected for histological analysis.

16s RNA sequencing

Sequencing of the bacterial 16s RNA was performed using the Microbial Systems Molecular Biology Lab which is part of the University of Michigan Host Microbiome Initiative. 8–12-week-old mice were given intraperitoneal injection of 100 mg/kg Tamoxifen (MP Biomedical, 156738) for 5 days. After 14 days of KO, mice were necropsied, and fecal pellets were collected from the intestines. Using a dual index sequencing strategy, the V4 regions of the 16s rRNA was amplified. The samples were then sequenced using MiSeq Reagent kit V2 500 cycles in Illkumia MiSeq. Mothur (v1.42.3) was used to analyze bacterial communities, and quality of the samples was demonstrated via aligned reading of a DNA extraction control and genotype clustering via principal component analysis.

qPCR

RNA was extracted for gene expression analysis from colon epithelial scrapes using the chloroform method. Samples were homogenized in Trizol (Ambion), the supernatant removed, and chloroform (Sigma-Aldrich) was used to cause phase separation. Isopropanol (Acros Organics) was added to cause RNA precipitation before the pellet was washed in 70% ethanol and allowed to dry before being reconstituted with water. RNA concentrations were measured using a nanodrop and synthesized into cDNA by Reverse Transcription. 1μg of RNA was loaded into each reaction including Oligo(dT) (Promega), dNTP mix (Thermo Scientific), and sterile water. Samples were heated at 65 ° for 6 minutes and quick chilled on ice prior to adding First strand buffer (Invitrogen) and DTT (Invitrogen) and incubating at 42°C for 2 minutes. SuperScript II RT (Invitrogen) was added to each reaction and incubated at 42°C for 50 minutes prior to enzyme inactivation by heating at 70°C for 15 minutes. RT-qPCR was performed using SYBR green master mix (Applied biosystems), cDNA, and forward and reverse primers. qPCR

cycles were run at a standard ramp speed and the resulting comparative ΔΔCT values were used to calculate gene expression between samples.

H&E

Samples were deparaffinized using xylene (Acros Organics) and rehydrated using washes of 100%, 95%, and 70% ethanol at room temperature. Slides were stained in Hematoxylin (Gill's 2x) (RICCA) for 2 minutes and dipped 1-2 times in bluing solution (ScyTek Laboratories). The slides were next counterstained in eosin and dehydrated using washes of 95% ethanol, 100% ethanol, and xylene. Coverslips were mounted onto slides using xylene based Permount (Fisher Chemical).

AB/PAS staining

Samples were deparaffinized using xylene (Acros Organics) and rehydrated using washes of 100% and 95% ethanol at room temperature. Samples were incubated in 3% acetic acid for 3 minutes followed by Alcian Blue (Newcomer Supply, 1003A) for 30 minutes at room temperature. Incubation in 0.5% periodic acid (brand) for 10 minutes was used to oxidize samples. Slides were next incubated in Schiff reagent (brand) at room temperature for 30 minutes. Samples were dehydrated using washes of 95% ethanol, 100% ethanol, and xylene. Coverslips were mounted onto slides using xylene based Permount (Fisher Chemical).

Western Blot

Upon necropsy, proximal colon epithelium was harvested and flash frozen in liquid nitrogen. Protein was extracted using RIPA buffer (Thermo Fisher) with protease and phosphatase inhibitors (Thermo Fisher). Protein concentration was quantified using a Pierce BSA protein assay kit (Thermo Fisher). Protein concentrations were normalized and samples for Western blot were prepared using RIPA buffer and loading dye to a final concentration of 4x. Samples were incubated at 95°C for 5 minutes prior to being flash frozen in liquid nitrogen and stored at -20°C until use. 6 μg of protein from each sample was loaded into a 4-20% Mini-PROTEAN® TGX gel (BioRad) and proteins were separated by size using electrophoresis. Gels were transferred onto a 0.45 μM nitrocellulose membrane by wet transfer method. Membranes were blocked in 5% milk for 1 hour at RT prior to incubation with primary antibodies (Muc2: 1:1000 from Proteintech, IRE1β: 1:500 and AGR2: 1:1000

from Invitrogen, and Fmo5: 1:1000 from Cell Signalling) overnight at 4°C. The following day, membranes were washed and incubated in anti-rabbit secondary antibody (company name) at a concentration of 1:1000 in 5% milk for 1 hour at RT. Proteins were visualized using an ECL kit (Thermo Fisher) and Chemidoc Imager before protein levels were analyzed using ImageJ.

TUDCA Treatment

Mice were given IP injection of 500 mg/kg/day of Tauroursodeoxycholic Acid (TUDCA, Cayman Chemical) dissolved in 1x PBS once daily starting 7 days prior to tamoxifen treatment. TUDCA treatment was continued during the tamoxifen treatment regime, where mice received an IP injection of each chemical for 5 days. Following the conclusion of tamoxifen treatment, mice received TUDCA injections for an additional 14 days and were euthanized at 14 days of KO.

REFERENCES

1. Johansson ME, Phillipson M, Petersson J, Velcich A, Holm L, Hansson GC. The inner of the two Muc2 mucin-dependent mucus layers in colon is devoid of bacteria. *Proc Natl Acad Sci U S A*. Sep 2008;105(39):15064-9. doi:10.1073/pnas.0803124105
2. Shin W, Kim HJ. Intestinal barrier dysfunction orchestrates the onset of inflammatory host-microbiome cross-talk in a human gut inflammation-on-a-chip. *Proc Natl Acad Sci U S A*. 11 06 2018;115(45):E10539-E10547. doi:10.1073/pnas.1810819115
3. Bischoff SC, Barbara G, Buurman W, et al. Intestinal permeability--a new target for disease prevention and therapy. *BMC Gastroenterol*. Nov 18 2014;14:189. doi:10.1186/s12876-014-0189-7
4. Ambort D, Johansson ME, Gustafsson JK, et al. Calcium and pH-dependent packing and release of the gel-forming MUC2 mucin. *Proc Natl Acad Sci U S A*. Apr 10 2012;109(15):5645-50. doi:10.1073/pnas.1120269109
5. Nilsson HE, Ambort D, Bäckström M, et al. Intestinal MUC2 mucin supramolecular topology by packing and release resting on D3 domain assembly. *J Mol Biol*. Jul 15 2014;426(14):2567-2579. doi:10.1016/j.jmb.2014.04.027
6. Specian RD, Neutra MR. Mechanism of rapid mucus secretion in goblet cells stimulated by acetylcholine. *J Cell Biol*. Jun 1980;85(3):626-40. doi:10.1083/jcb.85.3.626
7. Van der Sluis M, De Koning BA, De Bruijn AC, et al. Muc2-deficient mice spontaneously develop colitis, indicating that MUC2 is critical for colonic protection. *Gastroenterology*. Jul 2006;131(1):117-29. doi:10.1053/j.gastro.2006.04.020
8. Hanski C, Born M, Foss HD, et al. Defective post-transcriptional processing of MUC2 mucin in ulcerative colitis and in Crohn's disease increases detectability of the MUC2 protein core. *J Pathol*. Jul 1999;188(3):304-11. doi:10.1002/(SICI)1096-9896(199907)188:3<304::AID-PATH375>3.0.CO;2-A

9. Johansson ME, Gustafsson JK, Holmén-Larsson J, et al. Bacteria penetrate the normally impenetrable inner colon mucus layer in both murine colitis models and patients with ulcerative colitis. *Gut*. Feb 2014;63(2):281-91. doi:10.1136/gutjnl-2012-303207
10. Miki K, Moore DJ, Butler RN, Southcott E, Couper RT, Davidson GP. The sugar permeability test reflects disease activity in children and adolescents with inflammatory bowel disease. *J Pediatr*. Dec 1998;133(6):750-4. doi:10.1016/s0022-3476(98)70145-3
11. Leiser SF, Miller H, Rossner R, et al. Cell nonautonomous activation of flavin-containing monooxygenase promotes longevity and health span. *Science*. Nov 2015;doi:10.1126/science.aac9257
12. Phillips IR, Shephard EA. Drug metabolism by flavin-containing monooxygenases of human and mouse. *Expert Opin Drug Metab Toxicol*. Feb 2017;13(2):167-181. doi:10.1080/17425255.2017.1239718
13. Petalcorin MI, Joshua GW, Agapow PM, Dolphin CT. The fmo genes of Caenorhabditis elegans and C. briggsae: characterisation, gene expression and comparative genomic analysis. *Gene*. Feb 2005;346:83-96. doi:10.1016/j.gene.2004.09.021
14. Nicoll CR, Bailleul G, Fiorentini F, Mascotti ML, Fraaije MW, Mattevi A. Ancestral-sequence reconstruction unveils the structural basis of function in mammalian FMOs. *Nat Struct Mol Biol*. 01 2020;27(1):14-24. doi:10.1038/s41594-019-0347-2
15. The Human Protein Atlas-Fmo5. Accessed December 7th, 2021.
16. Gonzalez Malagon SG, Melidoni AN, Hernandez D, et al. The phenotype of a knockout mouse identifies flavin-containing monooxygenase 5 (FMO5) as a regulator of metabolic ageing. *Biochem Pharmacol*. Aug 2015;96(3):267-77. doi:10.1016/j.bcp.2015.05.013
17. Rera M, Clark RI, Walker DW. Intestinal barrier dysfunction links metabolic and inflammatory markers of aging to death in Drosophila. *Proc Natl Acad Sci U S A*. Dec 2012;109(52):21528-33. doi:10.1073/pnas.1215849110
18. Rose WA, Sakamoto K, Leifer CA. Multifunctional role of dextran sulfate sodium for in vivo modeling of intestinal diseases. *BMC Immunol*. Aug 01 2012;13:41. doi:10.1186/1471-2172-13-41
19. Wani KA, Goswamy D, Taubert S, Ratnappan R, Ghazi A, Irazoqui JE. NHR-49/PPAR-α and HLH-30/TFEB cooperate for. *Elife*. 05 12 2021;10doi:10.7554/eLife.62775
20. MacQueen AJ, Baggett JJ, Perumov N, et al. ACT-5 is an essential Caenorhabditis elegans actin required for intestinal microvilli formation. *Mol Biol Cell*. Jul 2005;16(7):3247-59. doi:10.1091/mbc.e04-12-1061
21. Choi HS, Bhat A, Howington MB, et al. FMO rewires metabolism to promote longevity through tryptophan and one carbon metabolism in C. elegans. *Nat Commun*. Feb 02 2023;14(1):562. doi:10.1038/s41467-023-36181-0
22. Lungaro L, Costanzini A, Manza F, et al. Impact of Female Gender in Inflammatory Bowel Diseases: A Narrative Review. *J Pers Med*. Jan 17 2023;13(2)doi:10.3390/jpm13020165
23. van der Flier LG, Clevers H. Stem cells, self-renewal, and differentiation in the intestinal epithelium. *Annu Rev Physiol*. 2009;71:241-60. doi:10.1146/annurev.physiol.010908.163145
24. Cheng H, Leblond CP. Origin, differentiation and renewal of the four main epithelial cell types in the mouse small intestine. V. Unitarian Theory of the origin of the four epithelial cell types. *Am J Anat*. Dec 1974;141(4):537-61. doi:10.1002/aja.1001410407
25. Bjerknes M, Cheng H. Clonal analysis of mouse intestinal epithelial progenitors. *Gastroenterology*. Jan 1999;116(1):7-14. doi:10.1016/s0016-5085(99)70222-2
26. Dignass AU. Mechanisms and modulation of intestinal epithelial repair. *Inflamm Bowel Dis*. Feb 2001;7(1):68-77. doi:10.1097/00054725-200102000-00014
27. Gregorieff A, Stange DE, Kujala P, et al. The ets-domain transcription factor Spdef promotes maturation of goblet and paneth cells in the intestinal epithelium. *Gastroenterology*. Oct 2009;137(4):1333-45.e1-3. doi:10.1053/j.gastro.2009.06.044

28. Nowarski R, Jackson R, Gagliani N, et al. Epithelial IL-18 Equilibrium Controls Barrier Function in Colitis. *Cell*. Dec 03 2015;163(6):1444-56. doi:10.1016/j.cell.2015.10.072
29. Asker N, Axelsson MA, Olofsson SO, Hansson GC. Dimerization of the human MUC2 mucin in the endoplasmic reticulum is followed by a N-glycosylation-dependent transfer of the mono- and dimers to the Golgi apparatus. *J Biol Chem*. Jul 24 1998;273(30):18857-63. doi:10.1074/jbc.273.30.18857
30. Ju T, Brewer K, D'Souza A, Cummings RD, Canfield WM. Cloning and expression of human core 1 beta1,3-galactosyltransferase. *J Biol Chem*. Jan 04 2002;277(1):178-86. doi:10.1074/jbc.M109060200
31. Neidhardt L, Cloots E, Friemel N, et al. The IRE1β-mediated unfolded protein response is repressed by the chaperone AGR2 in mucin producing cells. *EMBO J*. Mar 2024;43(5):719-753. doi:10.1038/s44318-023-00014-z
32. Imagawa Y, Hosoda A, Sasaka S, Tsuru A, Kohno K. RNase domains determine the functional difference between IRE1alpha and IRE1beta. *FEBS Lett*. Mar 05 2008;582(5):656-60. doi:10.1016/j.febslet.2008.01.038
33. Erben U, Loddenkemper C, Doerfel K, et al. A guide to histomorphological evaluation of intestinal inflammation in mouse models. *Int J Clin Exp Pathol*. 2014;7(8):4557-76.
34. Bernstein CN, Fried M, Krabshuis JH, et al. World Gastroenterology Organization Practice Guidelines for the diagnosis and management of IBD in 2010. *Inflamm Bowel Dis*. Jan 2010;16(1):112-24. doi:10.1002/ibd.21048
35. Tessner TG, Cohn SM, Schloemann S, Stenson WF. Prostaglandins prevent decreased epithelial cell proliferation associated with dextran sodium sulfate injury in mice. *Gastroenterology*. Oct 1998;115(4):874-82. doi:10.1016/s0016-5085(98)70259-8
36. Gajendran M, Loganathan P, Jimenez G, et al. A comprehensive review and update on ulcerative colitis. *Dis Mon*. Dec 2019;65(12):100851. doi:10.1016/j.disamonth.2019.02.004
37. McCormick DA, Horton LW, Mee AS. Mucin depletion in inflammatory bowel disease. *J Clin Pathol*. Feb 1990;43(2):143-6. doi:10.1136/jcp.43.2.143
38. Danese S, Fiocchi C. Ulcerative colitis. *N Engl J Med*. Nov 03 2011;365(18):1713-25. doi:10.1056/NEJMra1102942
39. Chen W, Zhuo M, Lu X, et al. SRC-3 protects intestine from DSS-induced colitis by inhibiting inflammation and promoting goblet cell differentiation through enhancement of KLF4 expression. *Int J Biol Sci*. 2018;14(14):2051-2064. doi:10.7150/ijbs.28576
40. Duckworth CA, Pritchard DM. Suppression of apoptosis, crypt hyperplasia, and altered differentiation in the colonic epithelia of bak-null mice. *Gastroenterology*. Mar 2009;136(3):943-52. doi:10.1053/j.gastro.2008.11.036
41. Luperchio SA, Schauer DB. Molecular pathogenesis of Citrobacter rodentium and transmissible murine colonic hyperplasia. *Microbes Infect*. Apr 2001;3(4):333-40. doi:10.1016/s1286-4579(01)01387-9
42. Scott F, Gonzalez Malagon SG, O'Brien BA, et al. Identification of Flavin-Containing Monooxygenase 5 (FMO5) as a Regulator of Glucose Homeostasis and a Potential Sensor of Gut Bacteria. *Drug Metab Dispos*. 09 2017;45(9):982-989. doi:10.1124/dmd.117.076612
43. Pullan RD, Thomas GA, Rhodes M, et al. Thickness of adherent mucus gel on colonic mucosa in humans and its relevance to colitis. *Gut*. Mar 1994;35(3):353-9. doi:10.1136/gut.35.3.353
44. Strugala V, Dettmar PW, Pearson JP. Thickness and continuity of the adherent colonic mucus barrier in active and quiescent ulcerative colitis and Crohn's disease. *Int J Clin Pract*. May 2008;62(5):762-9. doi:10.1111/j.1742-1241.2007.01665.x
45. Trabucchi E, Mukenge S, Baratti C, Colombo R, Fregoni F, Montorsi W. Differential diagnosis of Crohn's disease of the colon from ulcerative colitis: ultrastructure study with the scanning electron microscope. *Int J Tissue React*. 1986;8(1):79-84.

46. Kober OI, Ahl D, Pin C, Holm L, Carding SR, Juge N. γδ T-cell-deficient mice show alterations in mucin expression, glycosylation, and goblet cells but maintain an intact mucus layer. *Am J Physiol Gastrointest Liver Physiol*. Apr 01 2014;306(7):G582-93. doi:10.1152/ajpgi.00218.2013
47. Grey MJ, Cloots E, Simpson MS, et al. IRE1β negatively regulates IRE1α signaling in response to endoplasmic reticulum stress. *J Cell Biol*. Feb 03 2020;219(2)doi:10.1083/jcb.201904048
48. Shah SC, Khalili H, Gower-Rousseau C, et al. Sex-Based Differences in Incidence of Inflammatory Bowel Diseases-Pooled Analysis of Population-Based Studies From Western Countries. *Gastroenterology*. Oct 2018;155(4):1079-1089.e3. doi:10.1053/j.gastro.2018.06.043
49. Zhu J, Wang Z, Chen F, Liu C. Identification of genes and functional coexpression modules closely related to ulcerative colitis by gene datasets analysis. *PeerJ*. 2019;7:e8061. doi:10.7717/peerj.8061
50. Becker K, Jerchow B. Generation of Transgenic Mice by Pronuclear Microinjection" inAdvanced Protocols for Animal Transgenesis: An ISTT Manual. Generation of Transgenic Mice by Pronuclear Microinjection" inAdvanced Protocols for Animal Transgenesis: An ISTT Manual. Springer Protocols: Sroinger-Verlag; 2011. p. 99-116.
51. Williams JM, Duckworth CA, Vowell K, Burkitt MD, Pritchard DM. Intestinal Preparation Techniques for Histological Analysis in the Mouse. *Curr Protoc Mouse Biol*. Jun 01 2016;6(2):148-168. doi:10.1002/cpmo.2
52. Gurina TS, Simms L. Histology, Staining. StatPearls Publishing; 2023.
53. Matsuo K, Ota H, Akamatsu T, Sugiyama A, Katsuyama T. Histochemistry of the surface mucous gel layer of the human colon. *Gut*. Jun 1997;40(6):782-9. doi:10.1136/gut.40.6.782

ACKNOWLEDGEMENTS

We acknowledge Wanda Filipiak & Galina Gavrilina for preparation of transgenic mice in addition to the Transgenic Animal Model Core. Core support was provided by The University of Michigan Gut Peptide Research Center, NIH grant number DK34933. MLS was supported by NIH F31DK134183 and T32HD007505. SFL was supported by NIH P30AG024824 and the Glenn Foundation for Medical Research.

FIGURE LEGENDS

Figure 1. *fmo-2* mediates intestinal integrity and structure in *C. elegans*. (**A**) Diagram of Smurf assay. (**B**) Fluorescent images of wildtype (N2) worms fed Smurf-dyed food (OP50) at days 0, 3, 6, 10, and 13 of adulthood, and quantification of individual worm fluorescent intensity for each day, n = 15-18/condition. (**C**) Smurf assay of wildtype, *fmo-2* OE, and *fmo-2* KO worms at days 6 (n = 10-16/condition) and 10 of adulthood (n = 18-22/condition), and quantification of individual worm fluorescent intensity for each day. (**D***)* Fluorescent images of *fmo-2p::mCherry* worms following 20 hours of exposure to 5% DSS or M9 control, and quantification of individual worm fluorescent intensity, n = 14-18/condition. (**E**) Fluorescent images of ACT-5::GFP worms on Vector CTL or *fmo-2* RNAi, and quantification of individual worm fluorescent intensity, n = 17-20/condition. Quantification graphs display mean +/- SEM normalized to Day 0, wildtype, CTL, or Vector CTL, respectively. Statistical significance for **B** and **C** was calculated using Brown-Forsythe and Welch 1-way ANOVA tests adjusted for multiple comparisons. Significance for **D** and **E** was calculated using t-test with Welch's correction, two-tailed. * $p < 0.05$, ** $p < 0.01$, *** $p < 0.001$, ****$p < 0.0001$.

Figure 2. Fmo5 maintains crypt architecture in female mice. (**A**) Graphic of the organs where Fmo5 is expressed in mammals. (**B**) Diagram showing the design of the VillinER^{T2} cre^{+}; Fmo5$^{fl/fl}$ mouse line generation. (**C**) Relative gene expression of Fmo5 in colonic epithelium in Fmo5$^{+/+}$ and Fmo5$^{-/-}$ mice at 14 days after tamoxifen treatment, n = 4-5 mice/group. Statistical significance between groups was calculated using an unpaired t-test with Welch's correction, two-tailed. (**D**) Western blot of Fmo5 and β-actin proteins in colon epithelium and liver of Fmo5$^{+/+}$ and Fmo5$^{-/-}$ mice at 14 days of KO. (**E**) Representative H&E-stained images of proximal colons of female and male Fmo5$^{+/+}$ and Fmo5$^{-/-}$ mice after 14 days of KO. Scale bar = 100μm, 20x magnification. (**F**) Crypt length quantification (μm) of female and male Fmo5$^{+/+}$ and Fmo5$^{-/-}$ mice proximal colons represented in E. Each bar represents a single mouse where 40-50 crypts were measured. Error bars are displayed as mean+/-SEM of measurements from each

mouse (n = 5 mice/group). (**G, H**) Representative H&E-stained images of the proximal colon from female (**G**) and male (**H**) Fmo5$^{+/+}$ and Fmo5$^{-/-}$ mice at days 3-, 7-, and 10- of KO. Scale bar = 100μm, 20x magnification. (**I**, **J**) Crypt length quantification (μm) of female (**I**) and male (**J**) mice represented in G and H. Each bar represents a single mouse where 30-40 crypts were measured (n = 4-6 mice/group). All images taken at 20x magnification. A Nested 1-way ANOVA with multiple comparisons and Tukey post-hoc correction was performed for data in **F**, **I**, and **J** to determine statistical significance. Significant differences between groups is represented by: * $p < 0.05$, ** $p < 0.01$, *** $p < 0.001$, ****$p < 0.0001$.

Figure 3. Loss of Fmo5 impairs goblet cell migration. (**A**) Relative gene expression of Muc2 and Tff3 in colon epithelium of female and male Fmo5$^{+/+}$ and Fmo5$^{-/-}$ mice 14 days after tamoxifen treatment, n = 3-4 mice/group. (**B**) Immunofluorescence staining of Muc2 (green) and DAPI (blue) in female and male Fmo5$^{+/+}$ and Fmo5$^{-/-}$ proximal colons, 20x magnification (**C**) Experimental design of tamoxifen treatment and EdU labeling injection. (**D**) Representative images of Muc2 (magenta), EdU (green), and DAPI (blue) stained colons collected 24 hours after EdU labeling, 20x magnification. Scale bar = 100μm (**E**) Quantification of the height of EdU+ cells within the crypt and respective crypt length (μm) 24 hours after EdU labeling. Quantified proportion of EdU+ cell height normalized by each specific crypts' length, 10-25 crypts/mouse with each bar representing one mouse (n = 3 mice/group). (**F**) Relative gene expression of Klf4, Glfi1, and Spdef in colonic epithelium of female Fmo5$^{+/+}$ and Fmo5$^{-/-}$ mice, n = 4-5 mice/group. Unpaired t-tests with Welch's correction were used to calculate statistical significance between groups in **A**, **E**, and **F**. * $p < 0.05$.

Figure 4. Fmo5 KO decreases mucus barrier thickness. Representative images of AB/PAS-stained colon samples from female and male Fmo5$^{+/+}$ and Fmo5$^{-/-}$ mice at (**A**) day 14 of KO, (**B**) females at days 3-, 7-, and 10- of KO, and (**C**) males at days 3-, 7-, and 10- of KO. All images were taken at 20x magnification. Scale bar = 100μm. (**D**) Schematic of cross-sectional view of the colon with a healthy vs. dysfunctional mucus

barrier. (**E**) Representative images of colon cross-sections stained with AB/PAS and processed using Carnoy's fixative to preserve mucus barrier in female and male mice 14 days following tamoxifen treatment, 20x magnification. Scale bar = 100μm. Red arrows point to the inner mucus barrier. (**F**) Quantified inner mucus barrier thickness (μm) of images represented in F. ~30 measurements of inner mucus barrier thickness were made for each mouse (n = 3 mice/group), where each bar represents one mouse. Error bars display the mean +/-SEM for that mouse. Statistical significance was calculated using nested 1-way ANOVA with multiple comparisons and Tukey post-hoc correction. * $p < 0.05$, ** $p < 0.01$.

Figure 5. No evidence of dysbiosis in female Fmo5 KO mice. (**A**) Graph displaying bacterial 16s RNA sequencing of fecal pellets from female and male $Fmo5^{+/+}$ mice prior to tamoxifen treatment and female and male $Fmo5^{+/+}$ and $Fmo5^{-/-}$ mice after 13 days of KO. ♀=female, ♂=male. (**B**) Experimental design and timeline of tamoxifen and antibiotic treatment. (**C**) Representative images of H&E-stained colons from female and male $Fmo5^{+/+}$ and $Fmo5^{-/-}$ mice after 14 days of KO. Antibiotic treated mice were given a mixture of Gentamycin, Ampicillin, Neomycin, Penicillin, and Streptomycin in drinking water beginning at 5 days post-tamoxifen treatment. Mice were also gavaged with Vancomycin and Metronidazole (antibiotic treated) or PBS (CTL) every other day from 5-14 days of KO. 20x magnification, Scale bar = 100μm (**D, E**) Quantification of crypt length (μm) from (**D**) female and (**E**) male mice described in **C**. ~45-60 crypts were measured from the proximal colon of each mouse. Each bar represents one mouse (n = 4-5/group) and error bars reflect mean+/-SEM. Statistical significance was determined using a nested 1-way ANOVA with Tukey-corrected multiple comparisons. * $p < 0.05$, ** $p < 0.01$.

Figure 6. TUDCA treatment restores crypt length and mucus barrier thickness in female Fmo5 KO mice. (**A**) Relative gene expression of spliced- and total- xbp-1 in colon scrapes from female $Fmo5^{+/+}$ and $Fmo5^{-/-}$ mice 14 days post-tamoxifen treatment (n = 5 mice/group). The ratio of spliced to total xbp-1 was calculated for each mouse.

(**B**) Representative western blots of Agr2 and Ire-1β proteins with β-actin control from female Fmo5$^{+/+}$ and Fmo5$^{-/-}$ mice at 14 days of KO. (**C**) Quantification of Agr2 and Ire-1β protein levels described in **B**, normalized to their respective β-actin levels (n = 3-4). (D) Experimental design and timeline of TUDCA experiment. (**E**) Representative H&E-stained proximal colon from female Fmo5$^{+/+}$ and Fmo5$^{-/-}$ mice treated with TUDCA or PBS (CTL). 20x magnification, Scale bar = 100μm. (**F**) Crypt length (μm) quantification of samples represented in **E**. ~30 crypts were measured from each mouse, where each bar represents measurements from one mouse (5 mice/group). (**G**) AB/PAS-stained images of female mice +/- TUDCA treatment. 20x magnification, Scale bar = 100μm (**H**) Representative images of AB/PAS-stained colon cross-sections from TUDCA experiment that were processed using Carnoy's Fixative. 20x magnification, Scale bar = 100μm Red arrows highlight inner mucus barrier thickness. (**I**) Quantification of inner mucus barrier thickness (μm) represented in **H**. ~30 measurements were made for each mouse, and each bar shows data from one mouse (n = 5 mice/group). Statistical significance was calculated (**A, C)** using unpaired t-test with Welch's correction and (**F, I**) nested 1-way ANOVA with Tukey correction for multiple comparisons. * $p < 0.05$, ** $p < 0.01$, *** $p < 0.001$.

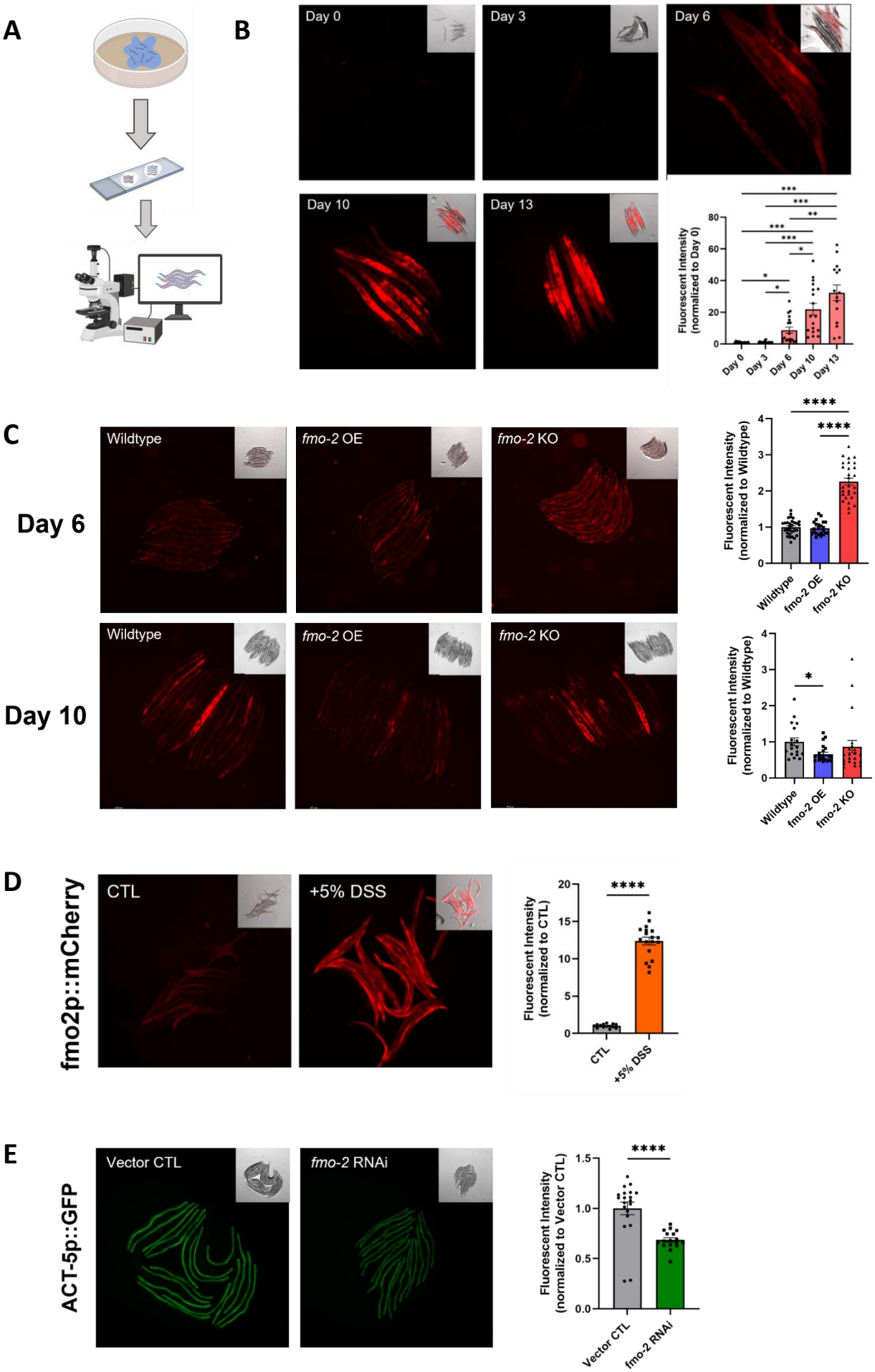
A
B
Day 0
Day 3
Day 6
Day 10
Day 13
Fluorescent Intensity (normalized to Day 0)
C
Day 6
Day 10
Wildtype
fmo-2 OE
fmo-2 KO
Fluorescent Intensity (normalized to Wildtype)
D
fmo2p::mCherry
CTL
+5% DSS
Fluorescent Intensity (normalized to CTL)
E
ACT-5p::GFP
Vector CTL
fmo-2 RNAi
Fluorescent Intensity (normalized to Vector CTL)

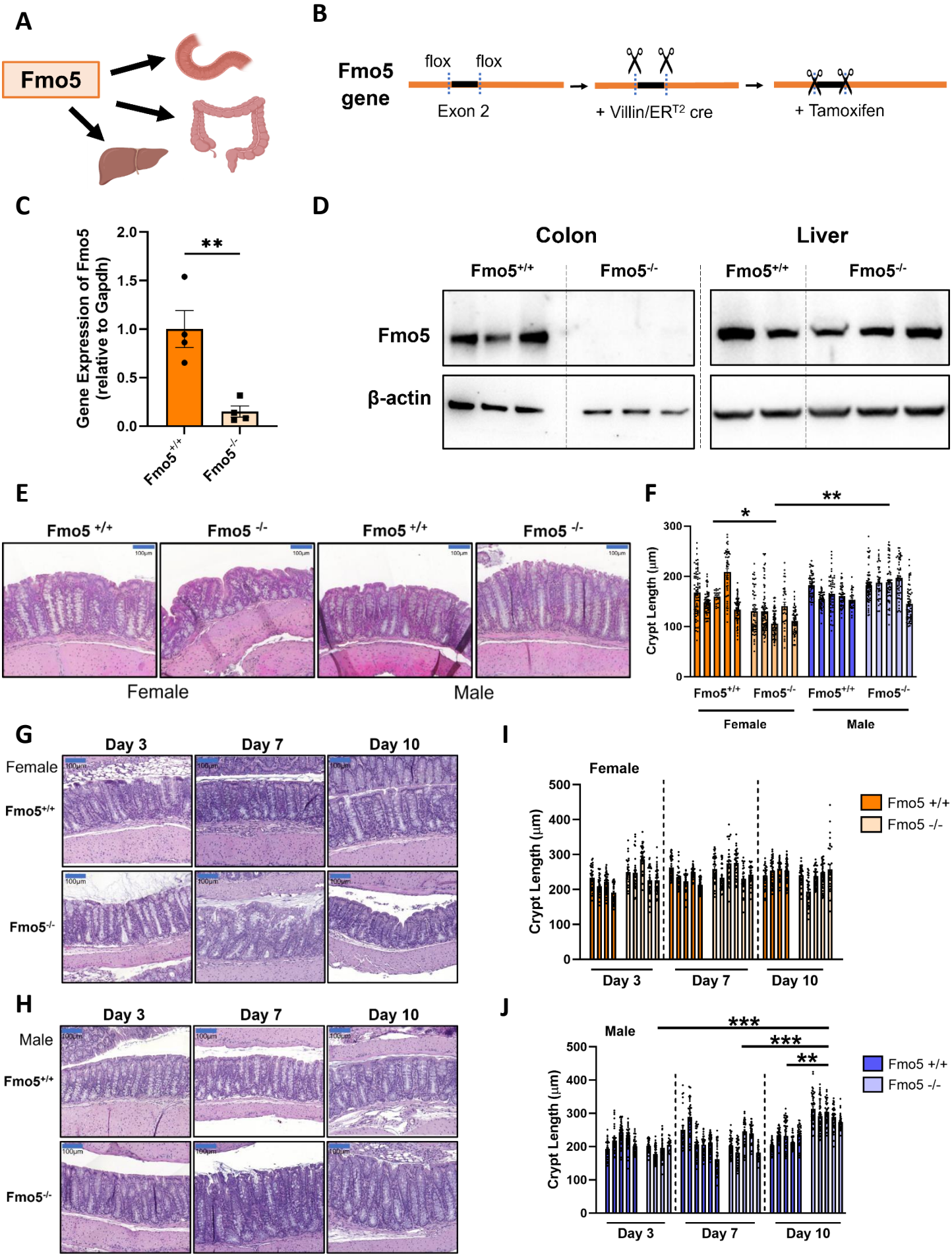
A
Fmo5
B
Fmo5 gene
flox
flox
Exon 2
+ Villin/ERT2 cre
+ Tamoxifen
C
Gene Expression of Fmo5 (relative to Gapdh)
2.0
1.5
1.0
0.5
0.0
**
Fmo5+/+
Fmo5-/-
D
Colon
Liver
Fmo5+/+
Fmo5-/-
Fmo5+/+
Fmo5-/-
Fmo5
β-actin
E
Fmo5 +/+
Fmo5 -/-
Fmo5 +/+
Fmo5 -/-
Female
Male
F
Crypt Length (μm)
300
200
100
0
*
**
Fmo5+/+
Fmo5-/-
Fmo5+/+
Fmo5-/-
Female
Male
G
Day 3
Day 7
Day 10
Female
Fmo5+/+
Fmo5-/-
H
Day 3
Day 7
Day 10
Male
Fmo5+/+
Fmo5-/-
I
Female
Crypt Length (μm)
500
400
300
200
100
0
Fmo5 +/+
Fmo5 -/-
Day 3
Day 7
Day 10
J
Male
Crypt Length (μm)
500
400
300
200
100
0
***
***
**
Fmo5 +/+
Fmo5 -/-
Day 3
Day 7
Day 10

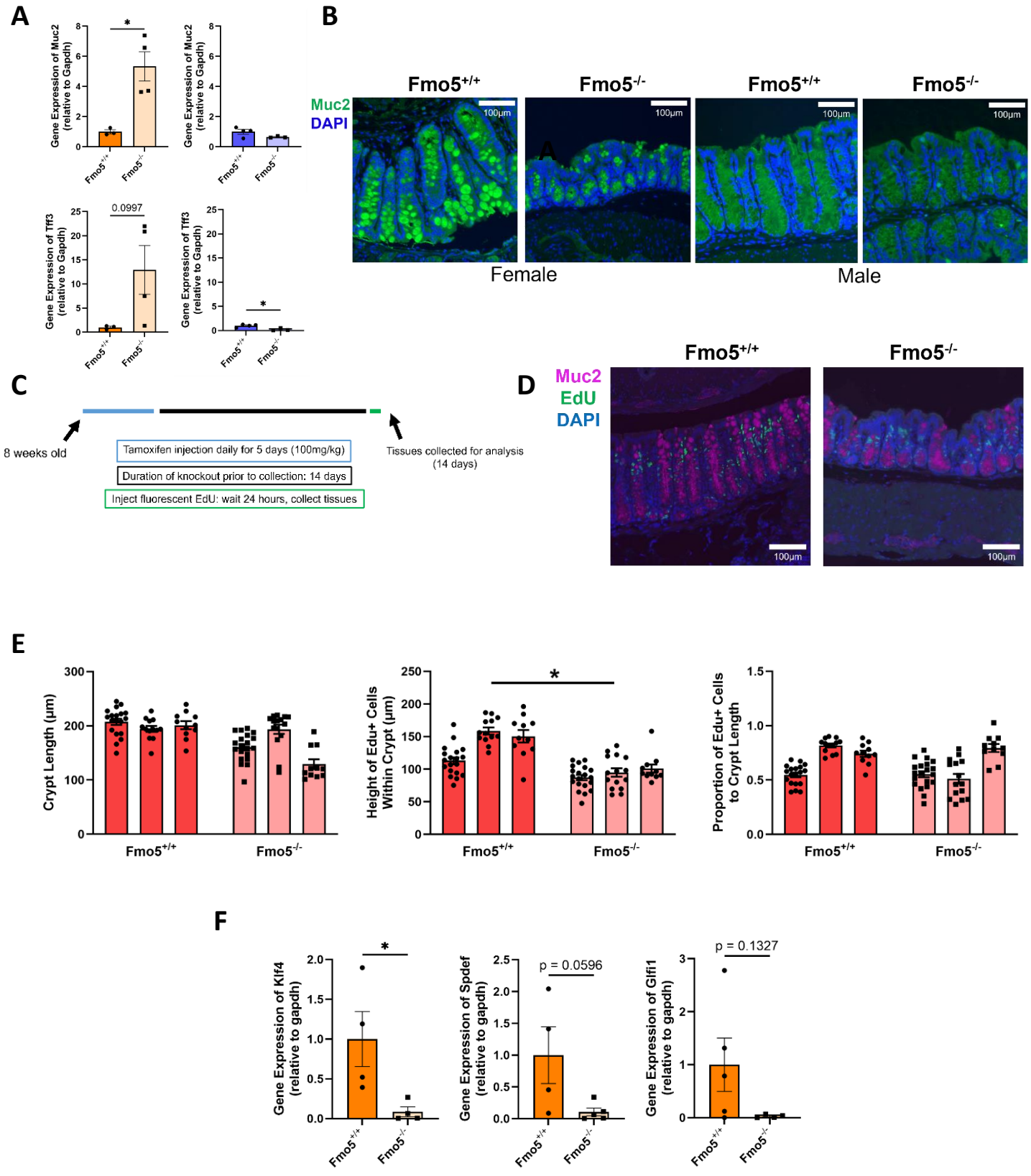
A
Gene Expression of Muc2 (relative to Gapdh)
Gene Expression of Tff3 (relative to Gapdh)
0.0997
Fmo5+/+
Fmo5-/-
B
Muc2
DAPI
Fmo5+/+
Fmo5-/-
100μm
Female
Male
C
8 weeks old
Tamoxifen injection daily for 5 days (100mg/kg)
Duration of knockout prior to collection: 14 days
Inject fluorescent EdU: wait 24 hours, collect tissues
Tissues collected for analysis (14 days)
D
Muc2
EdU
DAPI
E
Crypt Length (μm)
Height of Edu+ Cells Within Crypt (μm)
Proportion of Edu+ Cells to Crypt Length
F
Gene Expression of Klf4 (relative to gapdh)
Gene Expression of Spdef (relative to gapdh)
Gene Expression of Gfi1 (relative to gapdh)
p = 0.0596
p = 0.1327

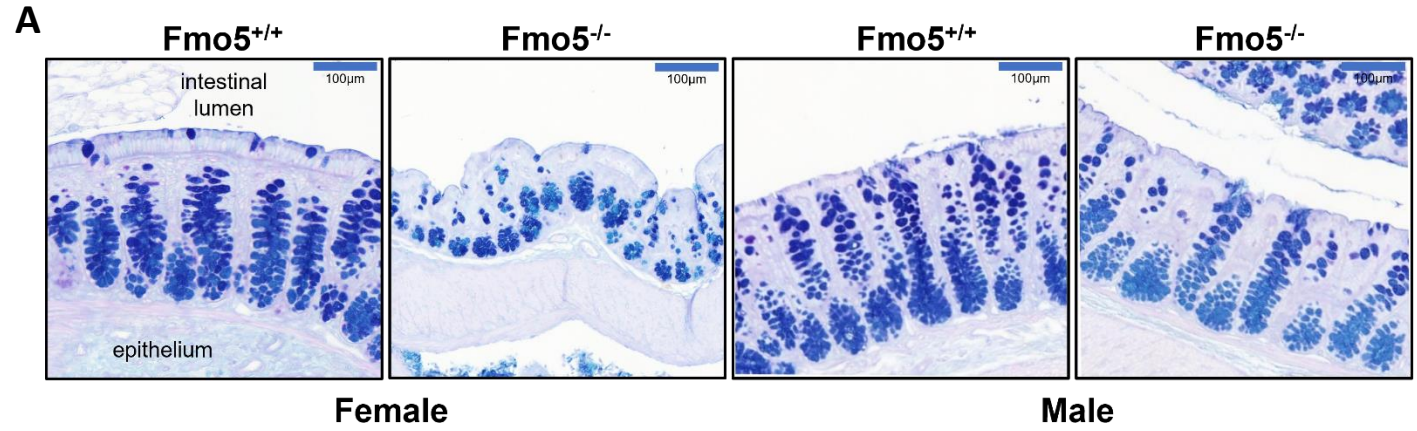
A
Fmo5+/+
Fmo5-/-
Fmo5+/+
Fmo5-/-
intestinal lumen
epithelium
100µm
Female
Male

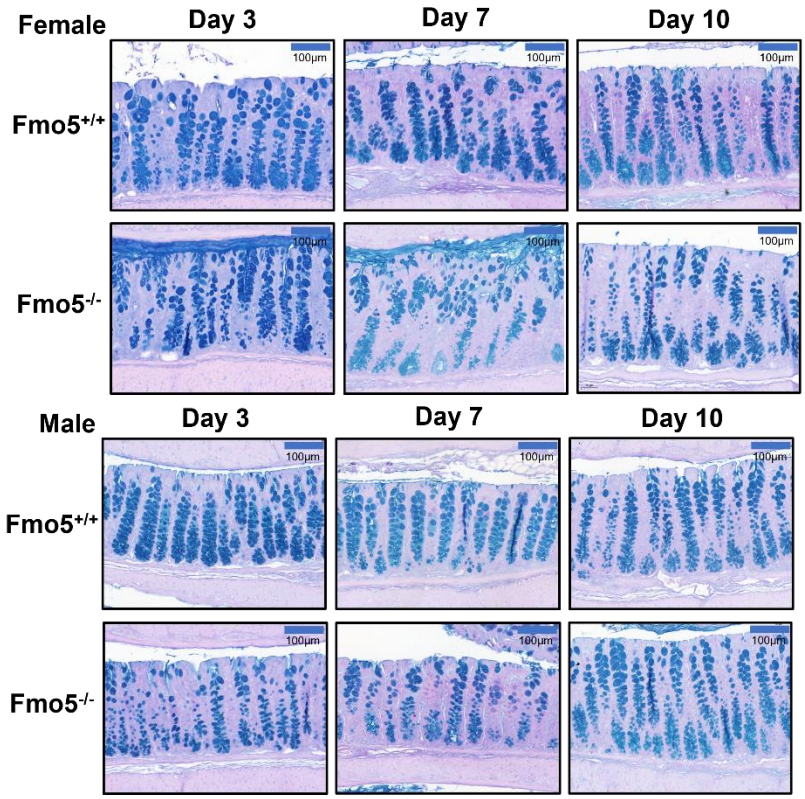
B
Female
Day 3
Day 7
Day 10
Fmo5+/+
Fmo5-/-
C
Male
Day 3
Day 7
Day 10
Fmo5+/+
Fmo5-/-
100µm

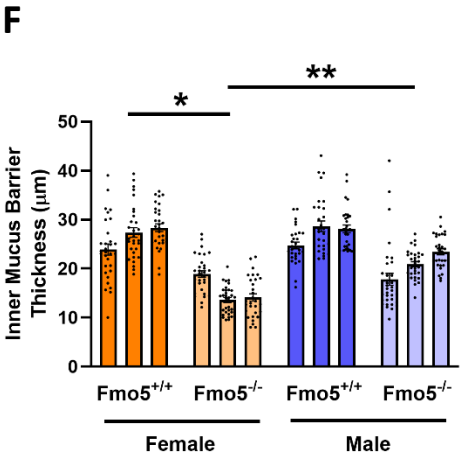
F
Inner Mucus Barrier Thickness (µm)
50
40
30
20
10
0
*
**
Fmo5+/+
Fmo5-/-
Fmo5+/+
Fmo5-/-
Female
Male

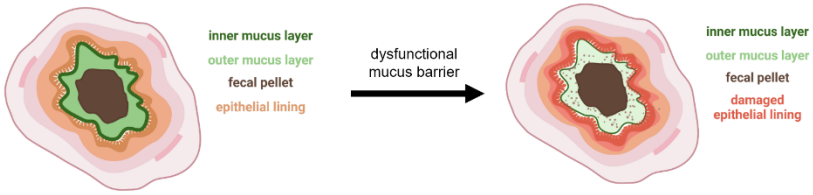
D
inner mucus layer
outer mucus layer
fecal pellet
epithelial lining
dysfunctional mucus barrier
inner mucus layer
outer mucus layer
fecal pellet
damaged epithelial lining

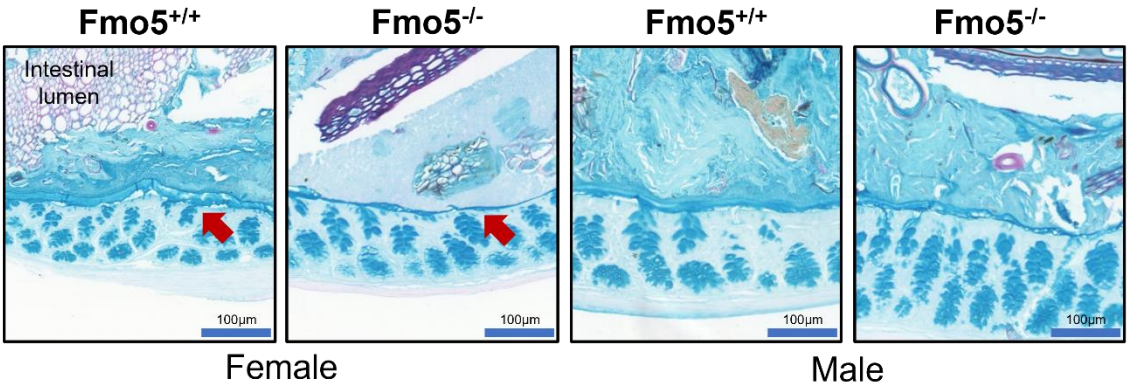
E
Fmo5+/+
Fmo5-/-
Fmo5+/+
Fmo5-/-
Intestinal lumen
100µm
Female
Male

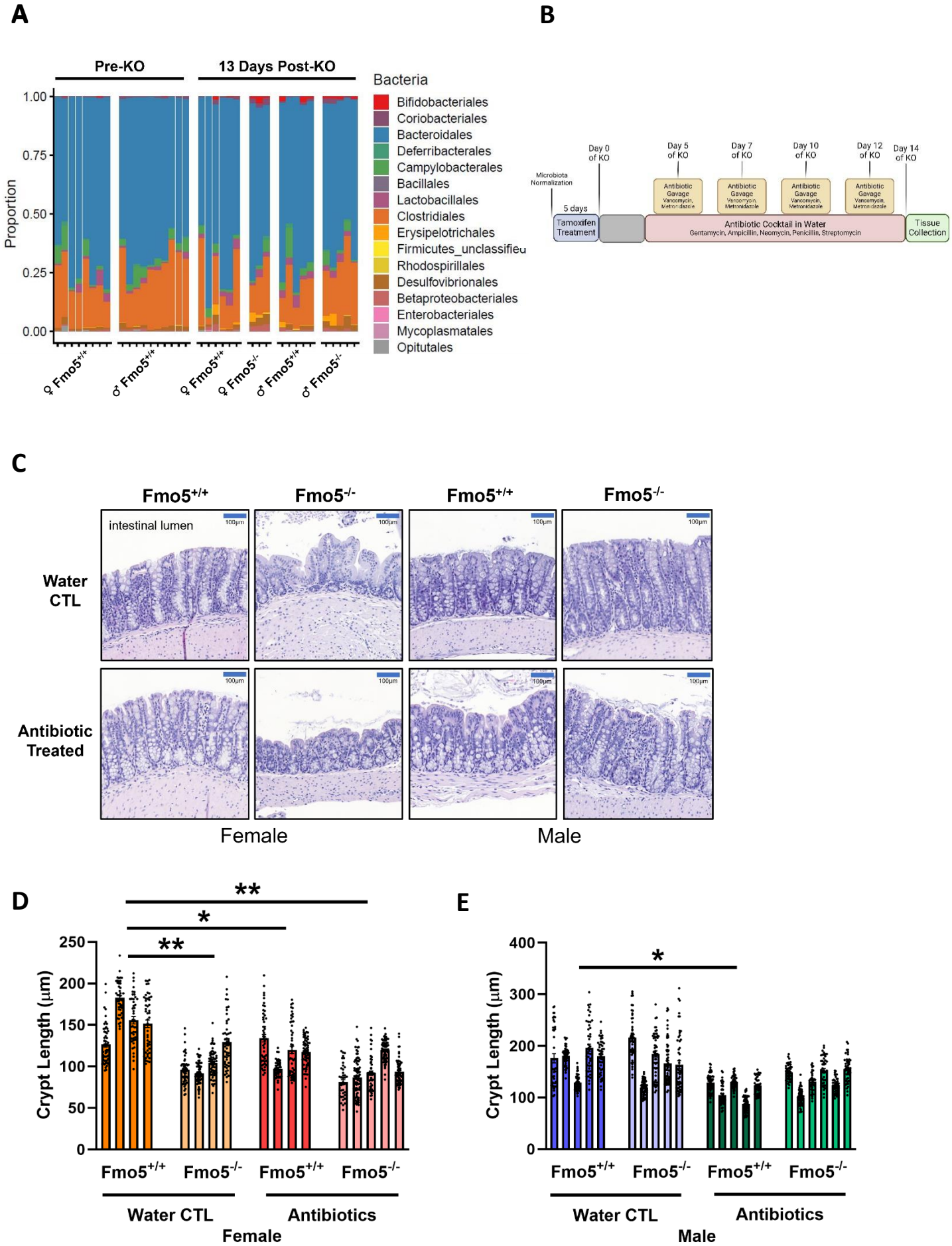
A
Pre-KO
13 Days Post-KO
Proportion
1.00
0.75
0.50
0.25
0.00
♀ Fmo5+/+
♂ Fmo5+/+
♀ Fmo5+/+
♀ Fmo5-/-
♂ Fmo5+/+
♂ Fmo5-/-
Bacteria
Bifidobacteriales
Coriobacteriales
Bacteroidales
Deferribacterales
Campylobacterales
Bacillales
Lactobacillales
Clostridiales
Erysipelotrichales
Firmicutes_unclassified
Rhodospirillales
Desulfovibrionales
Betaproteobacteriales
Enterobacteriales
Mycoplasmatales
Opitutales
B
Microbiota Normalization
5 days
Tamoxifen Treatment
Day 0 of KO
Day 5 of KO
Day 7 of KO
Day 10 of KO
Day 12 of KO
Day 14 of KO
Antibiotic Gavage Vancomycin, Metronidazole
Antibiotic Cocktail in Water
Gentamycin, Ampicillin, Neomycin, Penicillin, Streptomycin
Tissue Collection
C
Fmo5+/+
Fmo5-/-
Fmo5+/+
Fmo5-/-
intestinal lumen
100µm
Water CTL
Antibiotic Treated
Female
Male
D
Crypt Length (µm)
250
200
150
100
50
0
**
*
**
Fmo5+/+
Fmo5-/-
Fmo5+/+
Fmo5-/-
Water CTL
Antibiotics
Female
E
Crypt Length (µm)
400
300
200
100
0
*
Fmo5+/+
Fmo5-/-
Fmo5+/+
Fmo5-/-
Water CTL
Antibiotics
Male

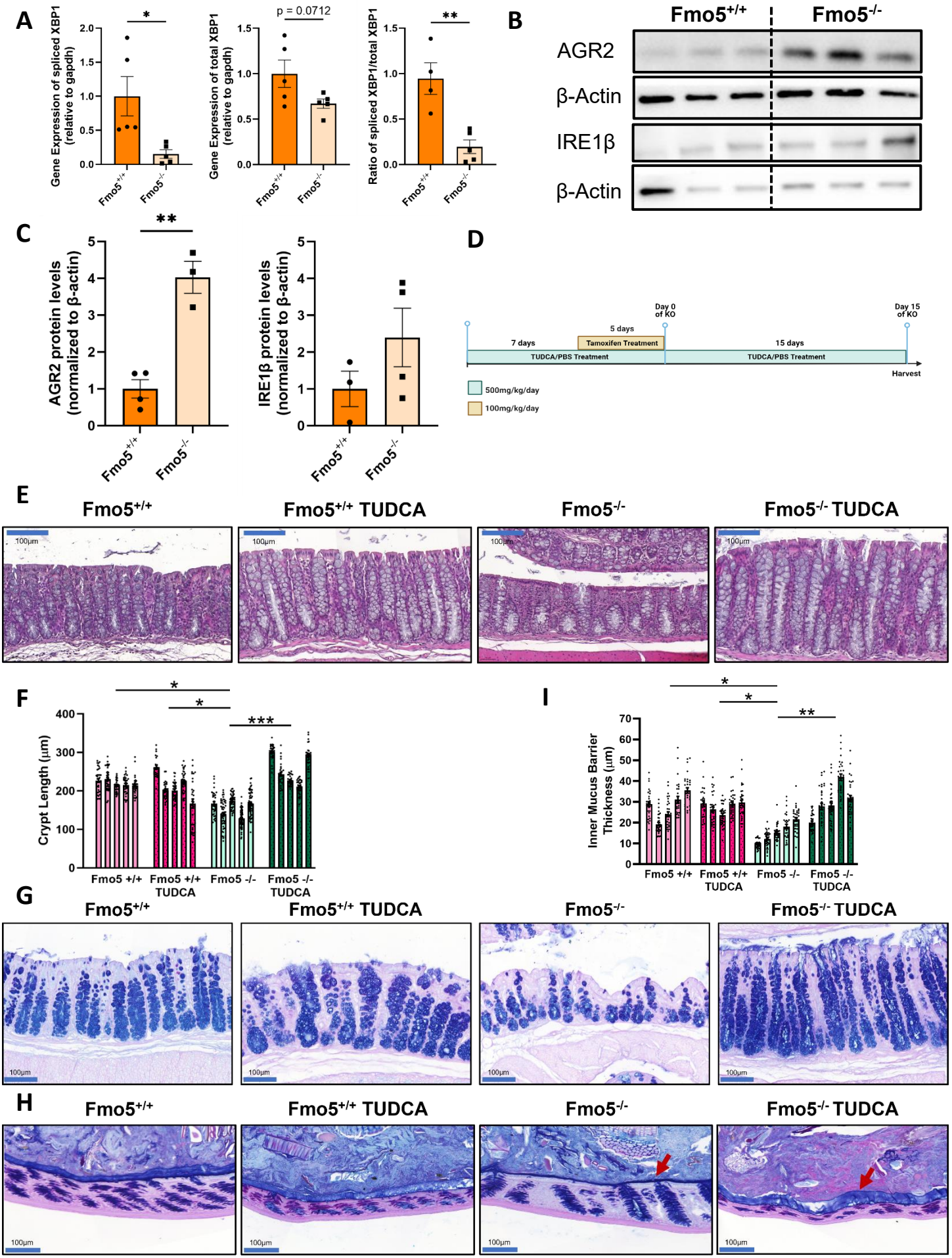
A
Gene Expression of spliced XBP1 (relative to gapdh)
Gene Expression of total XBP1 (relative to gapdh)
Ratio of spliced XBP1/total XBP1
p = 0.0712
Fmo5+/+
Fmo5-/-
B
Fmo5+/+
Fmo5-/-
AGR2
β-Actin
IRE1β
β-Actin
C
AGR2 protein levels (normalized to β-actin)
IRE1β protein levels (normalized to β-actin)
D
Day 0 of KO
Day 15 of KO
7 days
5 days
Tamoxifen Treatment
15 days
TUDCA/PBS Treatment
TUDCA/PBS Treatment
Harvest
500mg/kg/day
100mg/kg/day
E
Fmo5+/+
Fmo5+/+ TUDCA
Fmo5-/-
Fmo5-/- TUDCA
100μm
F
Crypt Length (μm)
Fmo5 +/+
Fmo5 +/+ TUDCA
Fmo5 -/-
Fmo5 -/- TUDCA
I
Inner Mucus Barrier Thickness (μm)
Fmo5 +/+
Fmo5 +/+ TUDCA
Fmo5 -/-
Fmo5 -/- TUDCA
G
Fmo5+/+
Fmo5+/+ TUDCA
Fmo5-/-
Fmo5-/- TUDCA
H
Fmo5+/+
Fmo5+/+ TUDCA
Fmo5-/-
Fmo5-/- TUDCA